Supporting Information

Phase Engineering of dual active 2D Bi_2O_3-based Nanosheets for Enhanced Alkaline Hydrogen Evolution Reaction Electrocatalysis

Ziyang Wu, Jun Mei, Qiong Liu, Sen Wang, Wei Li, Shihui Xing, Juan Bai, Jianping Yang, Wei Luo, Olga Guselnikova, Anthony P. O'Mullane, Yuantong Gu, Yusuke Yamauchi, Ting Liao, and Ziqi Sun**

***Corresponding Author**

E-mail: t3.liao@qut.edu.au (Ting Liao); ziqi.sun@qut.edu.au (Ziqi Sun)

Theoretical calculations: All calculations were performed within the spin-polarized density functional theory (DFT) framework as implemented in the Quantum-Espresso package. Ultrasoft pseudopotentials are introduced to describe the electron-ion interactions. Perdew-Burke-Ernzerhof (PBE) function in the generalized gradient approximation (GGA) was employed to describe the exchange-correlation functional. The Kohn-Sham (KS) orbitals and the charge density were represented using basis sets consisting of plane waves (PWs) up to a maximal kinetic energy of 50 Ry and 400 Ry, respectively. The Gibbs free energy of the adsorbed hydrogen atom is calculated by $\Delta G_H = \Delta E_H + \Delta E_{ZPE} - T\Delta S_H$. Where ΔEH is the adsorption energy of the hydrogen atom described above, and ΔE_{ZPE} is the zero-point energy correction for hydrogen adsorption. As for ΔS_H, it can be obtained by $\Delta S_H \cong -1/2 S_{H_2^0}$,, where $S_{H_2^0}$ is the entropy of a hydrogen molecule in the gas phase at the standard condition. Therefore, the overall corrections are expressed by $\Delta G_H = \Delta E_H + 0.24$, where 0.24 eV is the contribution from combination of ZPE and entropy at 298 K for surface models.

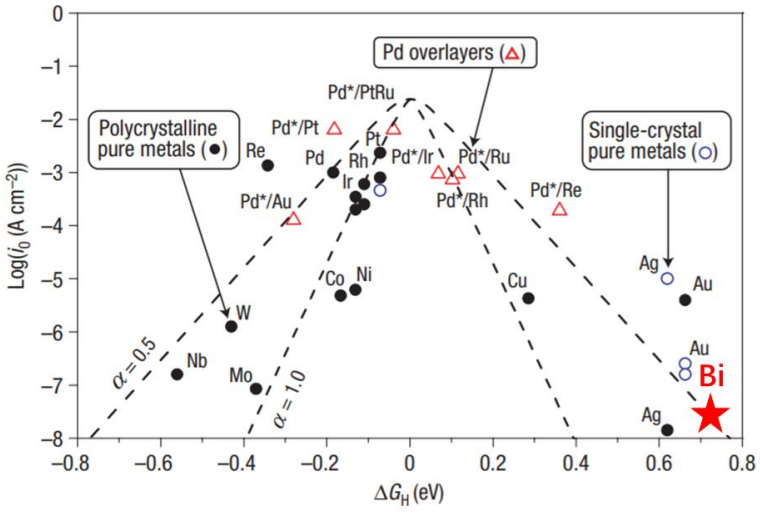

Figure S1. The calculated ΔG_{H^*} values of different pure metals and metal overlayers [1].

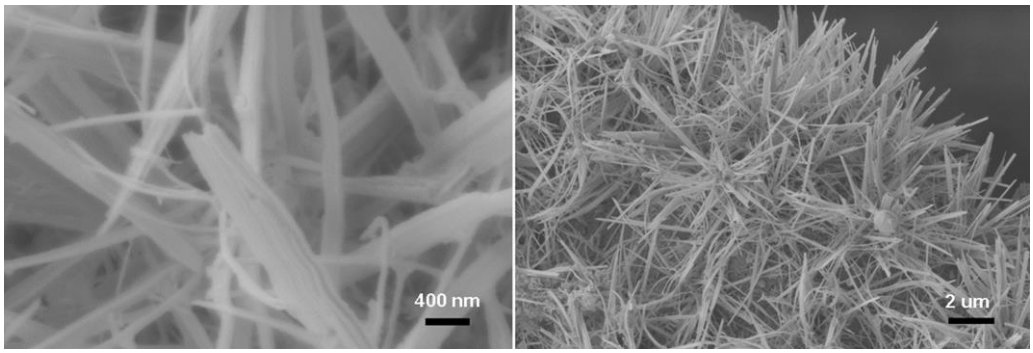

Figure S2. The SEM images of the sample RT without EG under different magnification. The scale bars are 400 nm and 2 μm, respectively.

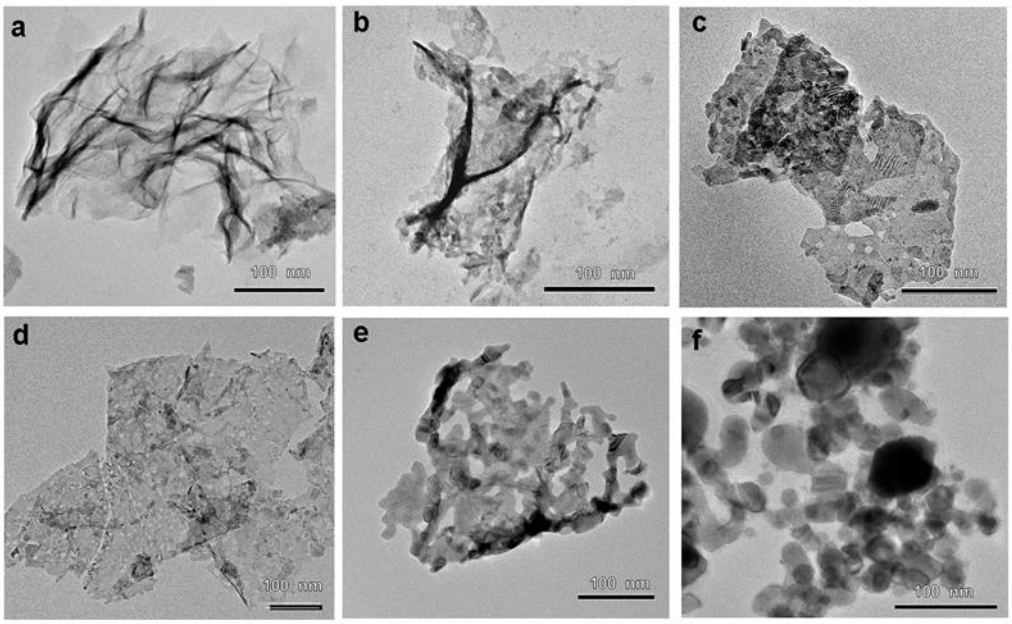

Figure S3. The low magnification of TEM images for sample RT, sample 400-Air, sample 200-H_2, sample 300-H_2, sample 400-H_2 and sample 500-H_2, respectively. The scale bars are 100 nm.

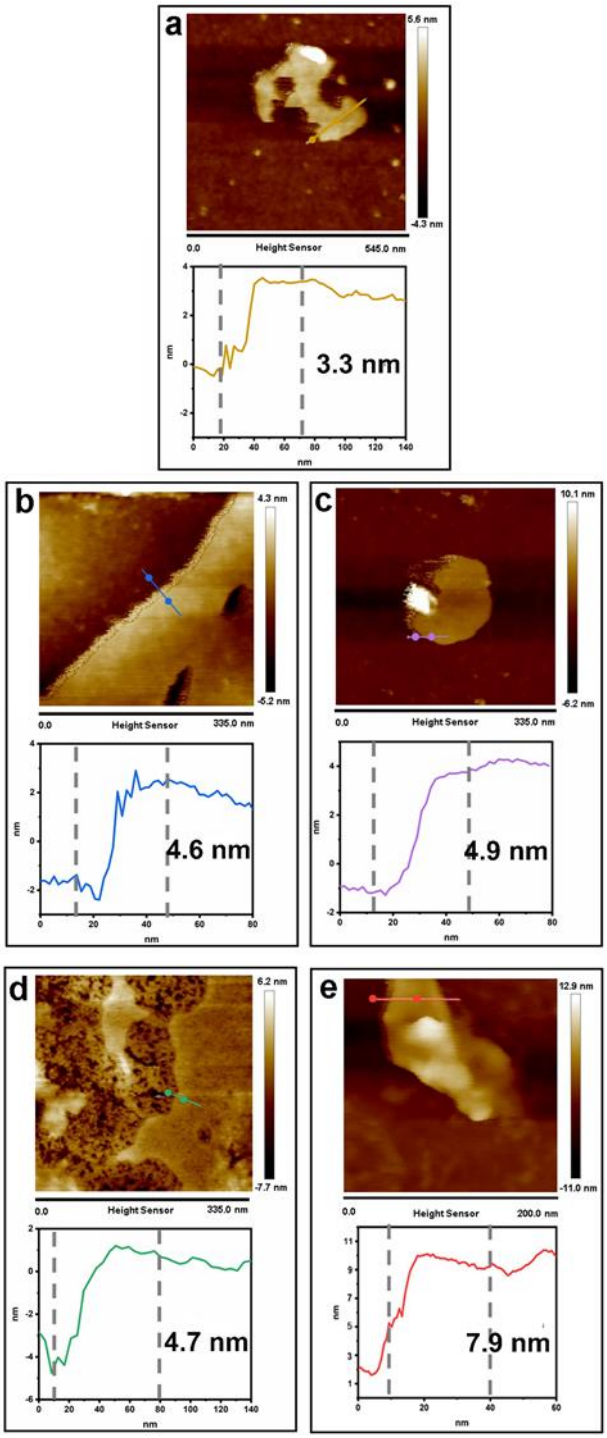

Figure S4. The AFM images of the (a) sample RT, (b) sample 400-Air, (c) sample 200-H_2, (d) sample 300-H_2, and (e) sample 400-H_2, respectively.

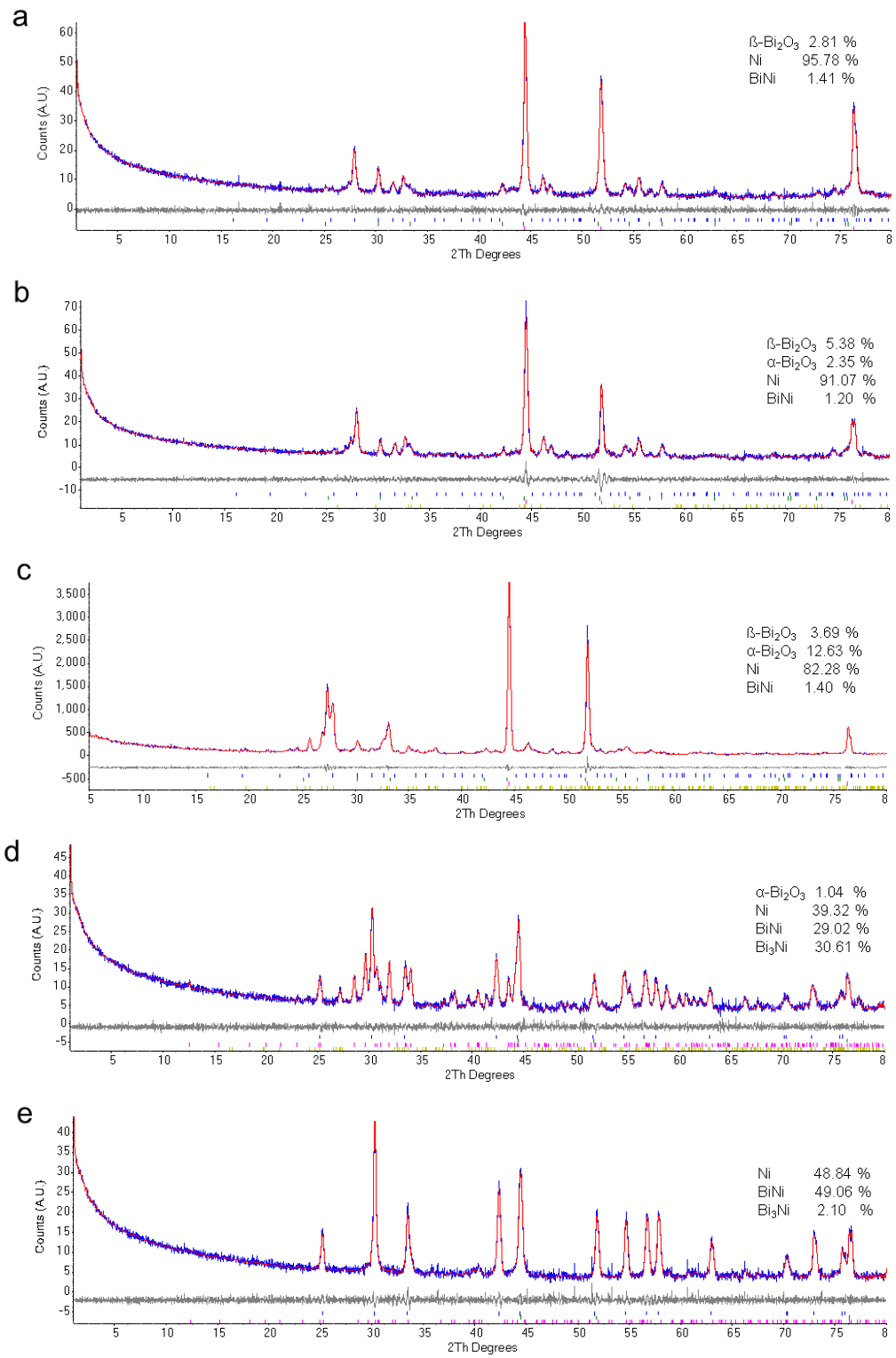

Figure S5. Rietveld refinement of the patterns of (a) 400-Air, (b) 200-H_2, (c) 300-H_2, (d) 400-H_2 and (e) 500-H_2.

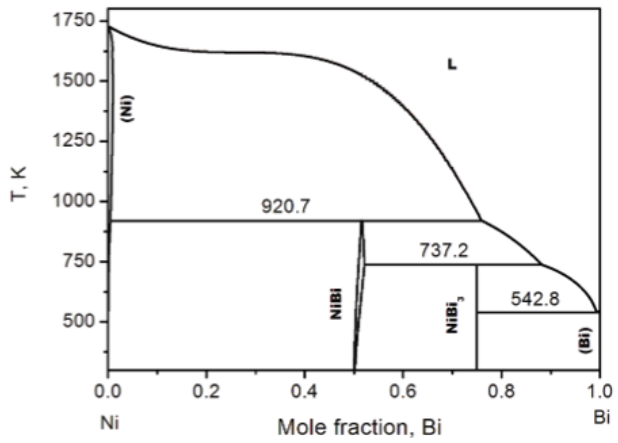

Figure S6. The Bi-Ni alloy phase diagram [2].

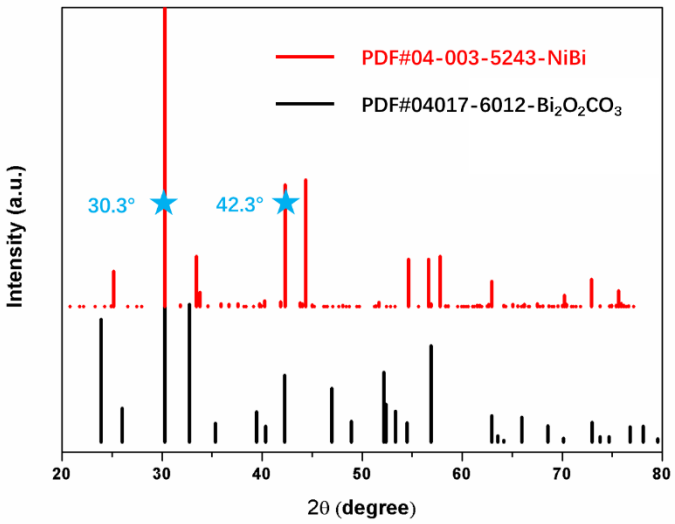

Figure S7. The XRD PDF patterns of NiBi and $Bi_2O_2CO_3$.

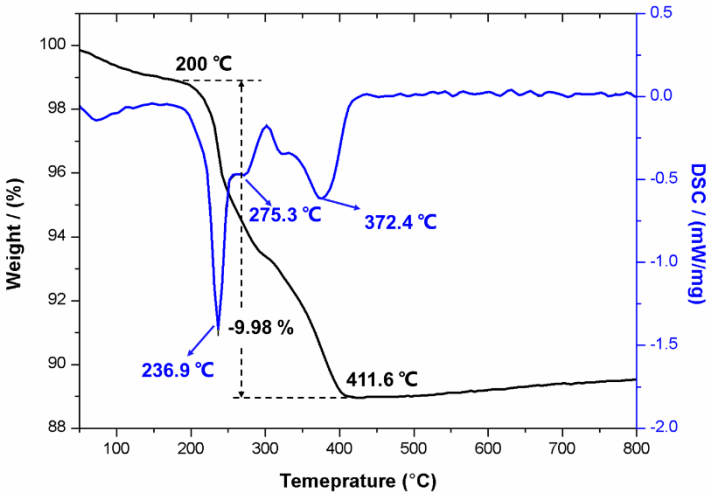

Figure S8. The thermogravimetric analysis (TGA) of $Bi_2O_2CO_3$ powder under air with a heating rate of 5 ℃/min.

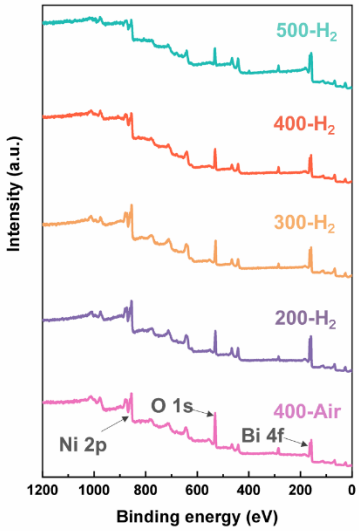

Figure S9. The wide scan spectrum of the prepared samples.

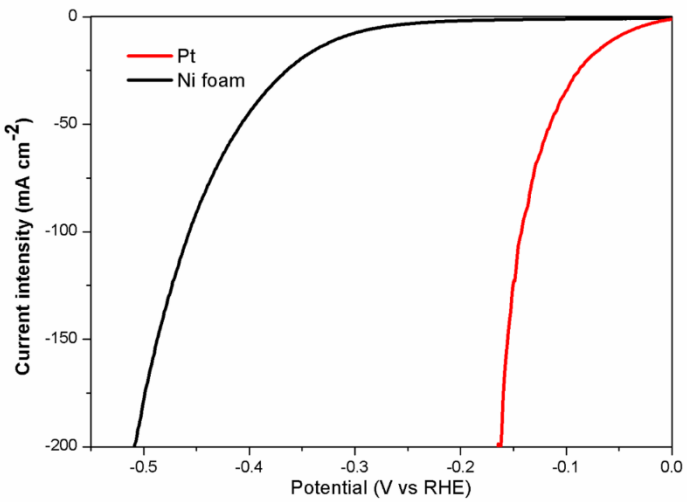

Figure S10. The polarization curves of bare Ni foam and Pt/C loaded Ni foam with a scan rate of 5 mV s^{-1}

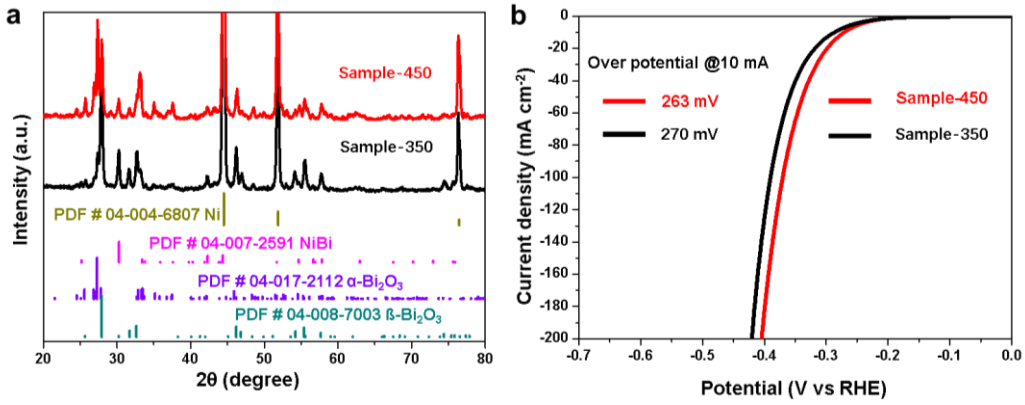

Figure S11. (a) The XRD data of sample-450 and sample 350 and (b) the polarization curves of different catalysts with a scan rate of 5 mV s^{-1} in 1.0 M KOH. Sample 350 and sample 450 were fabricated by the sample RT at 350 °C and 450 °C, respectively. As shown in the Figure11a, compared with sample-350, sample-450 demonstrated significantly increased α-Bi_2O_3 content, which can be characterized by the distinct peak position at and 27.9° and 27.3° for ß-Bi_2O_3 and α-Bi_2O_3, respectively. However, no significant HER difference was observed, also demonstrating the electrolytic improvement mainly stem from the phase engineering of alloy instead of phases change of Bi_2O_3.

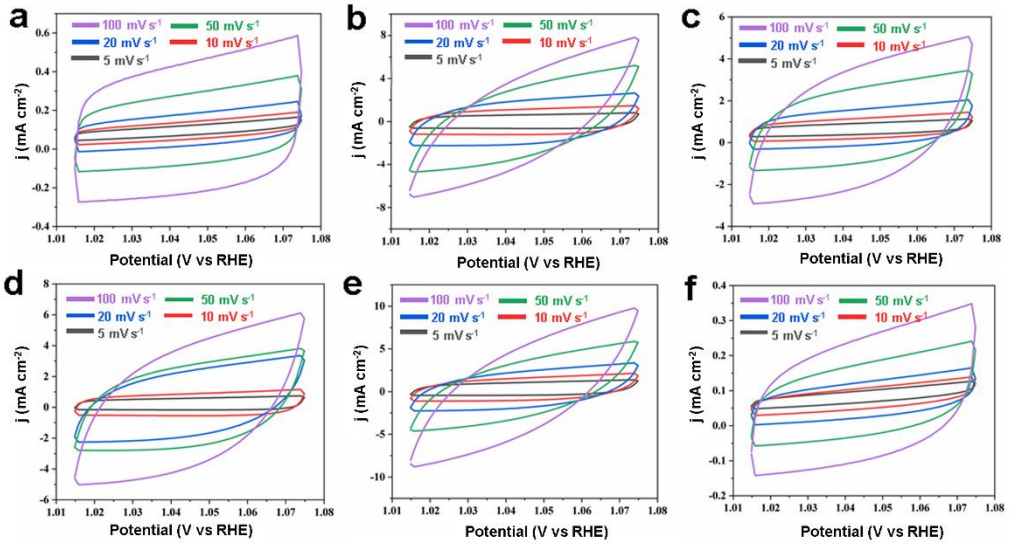

Figure S12. The cyclic voltammetry (CV) cycles in the region between 1.01 V and 1.08 V (vs. RHE) at different scan rates (5, 10, 20, 50 and 100 mv s^{-1}) of sample (a) RT, (b) 400-Air, (c) 200-H_2, (d) 300-H_2, (e) 400-H_2 and (f) 500-H_2.

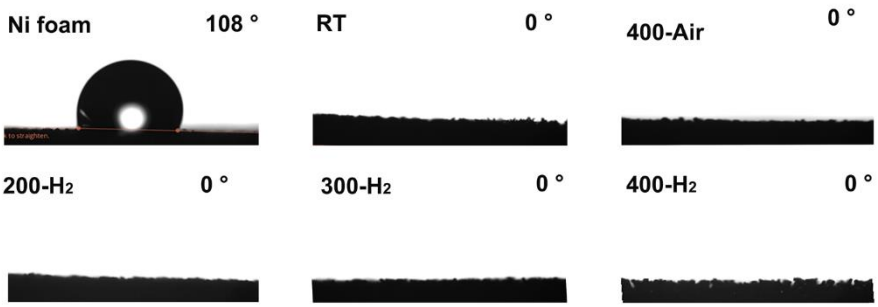

Figure S13. The water contact angle (5 μL) of different samples.

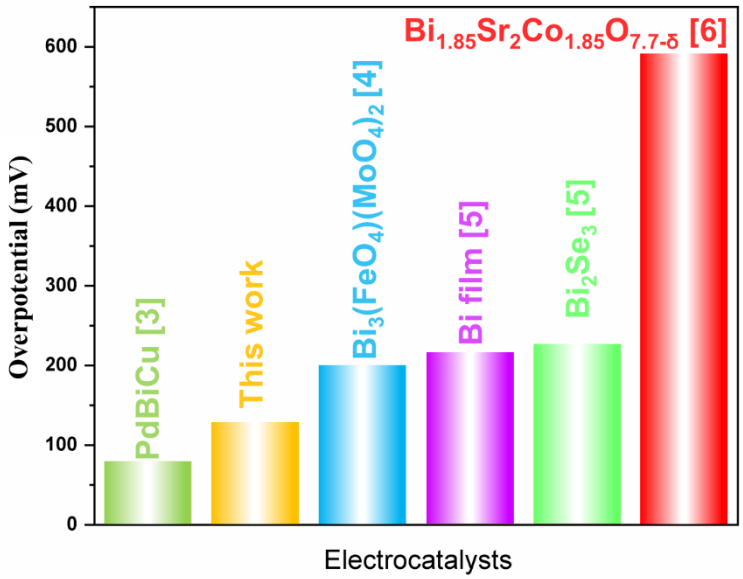

Figure S14. Comparison of the overpotentials required to reach the current density of 10 mA cm^{-2} among the reported Bismuth-based electrocatalysts [3-6]. Notes: as very few Bismuth based electrocatalysts was employed for alkaline HER, the referredces cited here (3 and 6) were tested under acid condition.

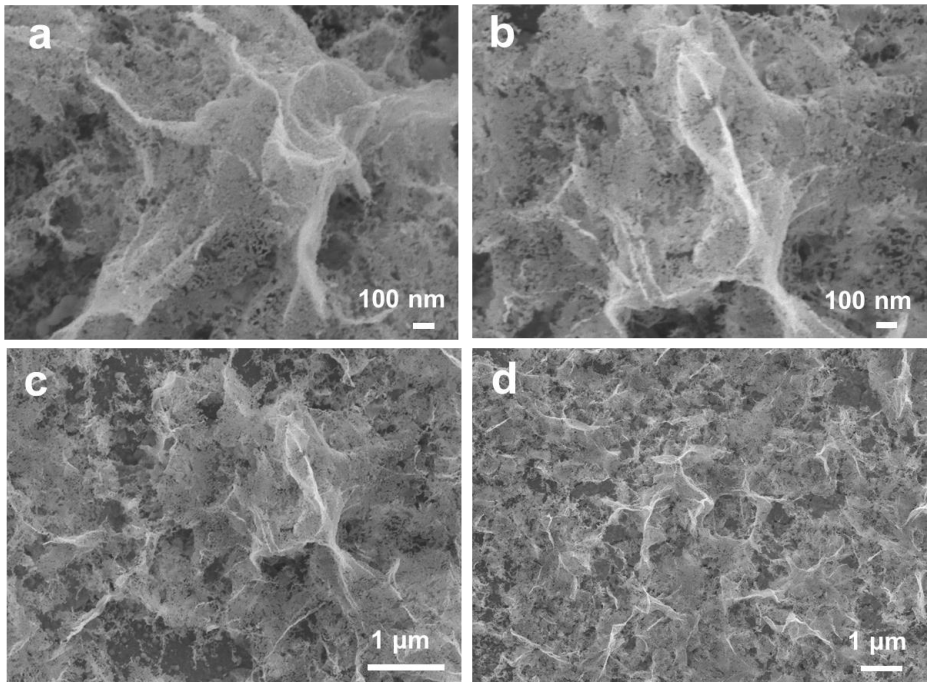

Figure S15. The SEM images of the 400-H_2 sample after the HER operation.

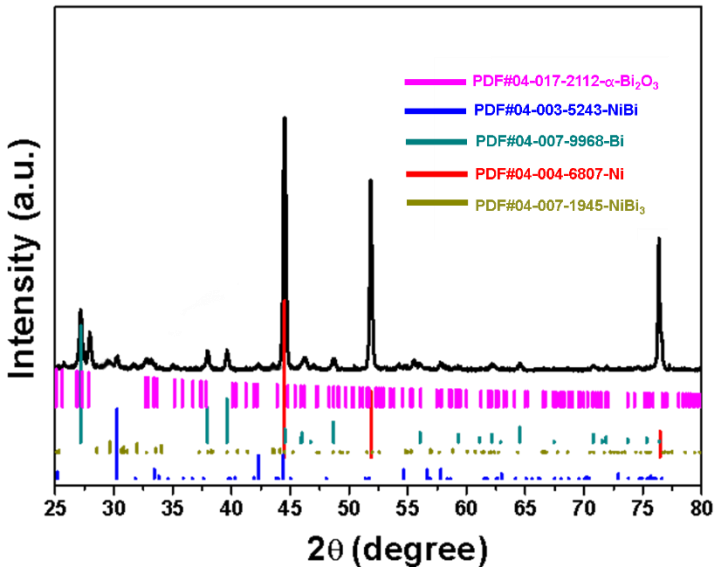

Figure S16. The XRD patterns of the 400-H_2 sample after the HER operation. It should be noted Bi metal formed after the long time HER operation as well as the existence of NiBi $NiBi_3$ and α-Bi_2O_3.

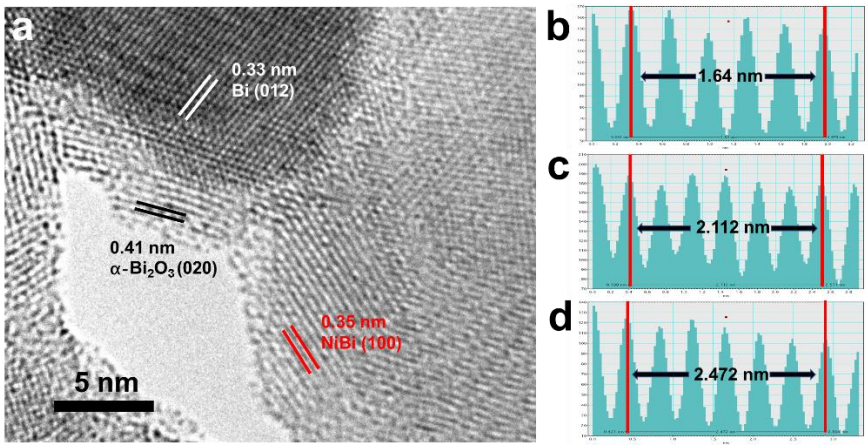

Figure S17. (a) The high-resolution TEM images of the 400-H_2 sample after the HER operation and the intensity line profile of the HRTEM images of (b) Bi (012), (c) NiBi (100) and (d) α-Bi_2O_3 (020)

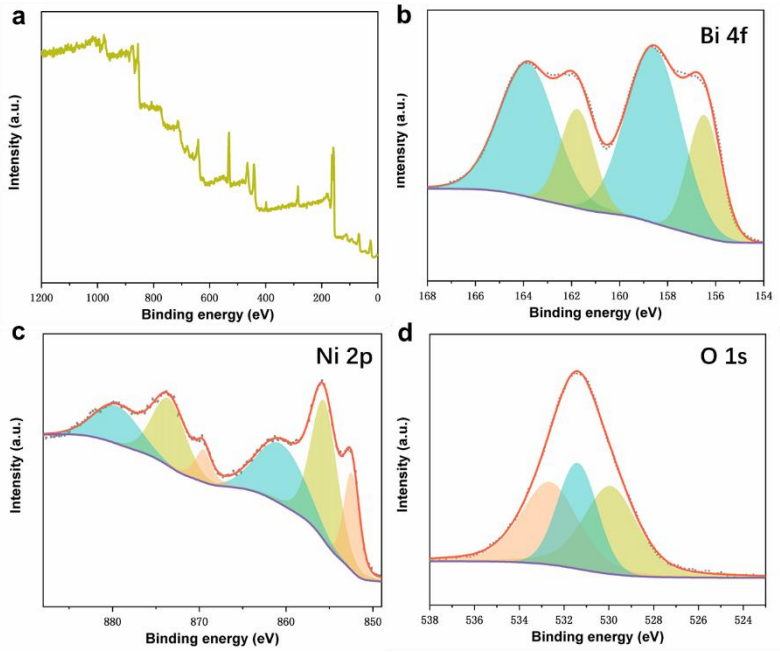

Figure S18. The XPS images of the 400-H_2 sample after the HER operation.

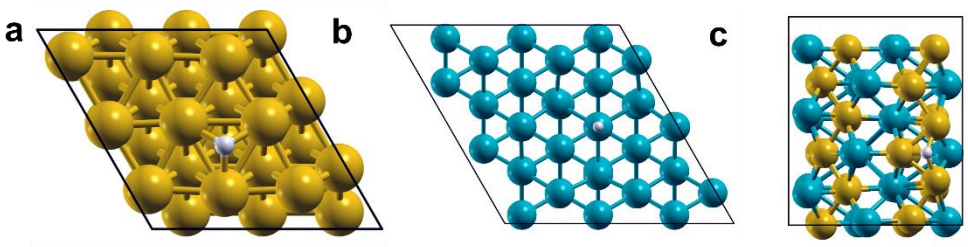

Figure S19. The schematic views of (a) Ni, (b) Bi, and (c) BiNi.

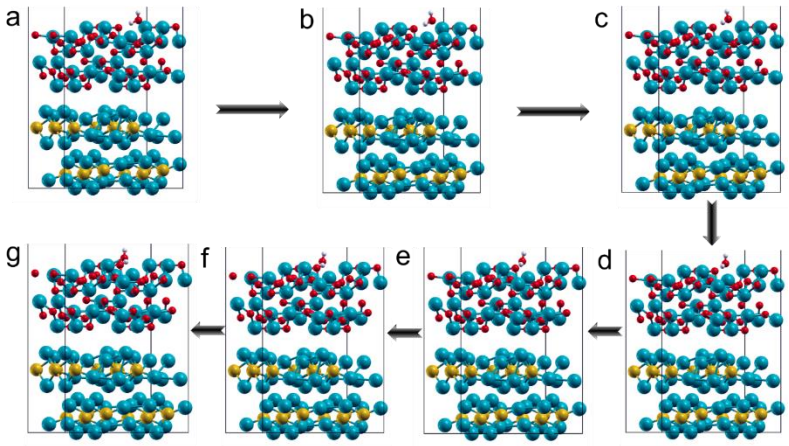

Figure S20. The detailed process of the water adsorption steps on to the Bi_2O_3&Bi_3Ni catalysts surface with DFT.

Table S1. The calculated contents of different phases from the XRD data of sample 400-Air, sample 200-H_2, sample 300-H_2, sample 400-H_2 and sample 500-H_2, respectively.

	Nickel (%)	**α-Bi_2O_3 (%)**	**ß-Bi_2O_3 (%)**	**BiNi (%)**	**Bi_3Ni(%)**
400-Air	95.78		2.81	1.41	
200-H_2	91.07	2.35	5.38	1.20	
300-H_2	82.28	12.63	3.69	1.40	
400-H_2	39.32	1.04		29.02	30.61
500-H_2	48.84			49.06	2.10

Table S2. The ratio of the content of Ni and Bi calculated from XPS for different samples.

	Nickel (%)	**Bi (%)**	**Bi^{3+} (%)**	**Bi^{0} (%)**	**O (%)**	**C (%)**
400-Air	21.29	7.89	100		46.48	24.34
200-H_2	21.96	6.25	100		46.14	25.65
300-H_2	14.69	5.42	100		42.05	37.84
400-H_2	11.38	10.06	70.17	29.83	37.88	40.68
500-H_2	8.67	13.01	48.91	51.09	35.47	42.85

Table S3. The of calculated resistance values of ohmic resistance (R_s) and charge transfer resistance (R_{ct}).

	RT	**400-Air**	**200-H_2**	**300-H_2**	**400-H_2**	**500-H_2**
R_s	2.1	2.18	2	2.17	2.12	2.24
R_{ct}	6.21	3.47	4.05	3.96	2.59	6.69

References

1. J. Greeley, T.F. Jaramillo, J. Bonde, I. Chorkendorff, J.K. Nørskov, *Nat. Mater*. **2006**, *5*, 909-913.
2. G. Vassilev, V. Gandova, P. Docheva, *Cryst. Res. Technol.* **2009**, *44*, 25-30.
3. L. Zheng, S. Zheng, H. Wei, L. Du, Z. Zhu, J. Chen, D. Yang, *ACS Appl. Mater. Interfaces*, **2019**, *11*, 6248-6256.
4. S. Khatun, P. Roy, *Chem. Commun*. **2020**, *56*, 7293-7296.
5. S. Razzaque, M.D. Khan, M. Aamir, M. Sohail, S. Bhoyate, R.K. Gupta, M. Sher, J. Akhtar, N. Revaprasadu, *Inorg. Chem.* **2021**, *60*, 1449-1461.
6. C.K. Chua, Z. Sofer, O. Jankovský, M.J.C. Pumera, *ChemPhysChem* **2015**,*16*, 769-774.